

Development and Characterization of CO₂–Responsive Intelligent Polymer Sealant

Published as part of the ACS Omega virtual special issue “CO₂ Geostorage”.

Huimei Wu,* Yishan Lou, Xiaopeng Zhai, Zhonghui Li, and Bin Liu



Cite This: *ACS Omega* 2023, 8, 35066–35076



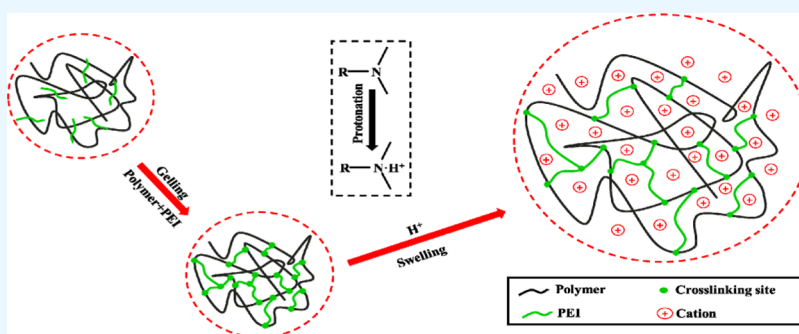
Read Online

ACCESS |

Metrics & More

Article Recommendations

Supporting Information



ABSTRACT: In this study, we present an innovative intelligent polymer sealant designed to mitigate CO₂ leakage during underground geological storage (CCUS). This sealant is formulated by cross-linking CO₂-responsive polymers, specifically acrylamide (AM) and N-[3-(dimethylamino) propyl] methacrylamide (DMAPMA), with polyethylenimine (PEI) serving as the cross-linking agent. The polymer sealant's characteristics were systematically investigated, varying the CO₂-responsive polymer content (1.5 wt %) and PEI content (0.1–0.6 wt %). A comprehensive analysis encompassing the rheological properties, thermal behavior, conductivity, and microstructures was conducted. Experimental results indicate that the polymer sealant exhibits excellent injectability, rapid response kinetics, thermal stability, and robust mechanical strength. Upon encountering CO₂, the polymer system undergoes a transition from sol to gel state, forming a surface-smooth, uniformly porous three-dimensional (3D) network skeleton structure. Remarkably, the gel's modulus remains relatively unaffected by the shear frequency. Core fluid displacement experiments demonstrated a substantial sealing efficiency of 73.6% for CO₂ and an impressive subsequent injection water sealing rate of 96.2%, underscoring its superior sealing and migration performance. In conclusion, the proposed CO₂-responsive gel sealant exhibits an exceptional potential for successful utilization in CCUS operations. This advancement introduces a novel avenue to enhance the effectiveness of CO₂-responsive gel sealants, thereby contributing to the advancement of CO₂ leakage mitigation strategies in geological storage scenarios.

1. INTRODUCTION

In the pursuit of low-carbon utilization of fossil energy, the technology of capturing, utilizing, and storing CO₂ (CCUS) holds paramount importance. Nonetheless, challenges related to CO₂ leakage or escape during geologic storage have arisen.^{1,2} Consequently, the imperative task of ensuring long-term storage safety has emerged as a pivotal concern requiring immediate attention within the domain of CCUS technology.

CO₂ storage serves as a method for mitigating atmospheric CO₂ concentration, with the prevalent approach involving the injection of CO₂ sealants into geological formations.³ Traditional CO₂ sealants often require elevated temperature and pressure, known as physical sealants for CO₂ entrapment. However, chemical sealants can pose environmental challenges and pollution risks.^{4–6} In contrast, pH-responsive polymer gel systems exhibit favorable attributes such as low viscosity and

robust flowability. They can infiltrate micropores inaccessible to conventional cement particles, establishing an impermeable isolation barrier. This characteristic, along with its sealing proficiency and stability, effectively prevents CO₂ leakage and escape during geologic storage.^{7–9} Notably, the CO₂-responsive intelligent gel sealing system represents a prominent category within pH-responsive polymer gels. This system swells in acidic conditions, bolstering its sealing efficacy.¹⁰ Recent research highlights the capability of polyacrylamide gels

Received: June 26, 2023

Accepted: August 30, 2023

Published: September 11, 2023



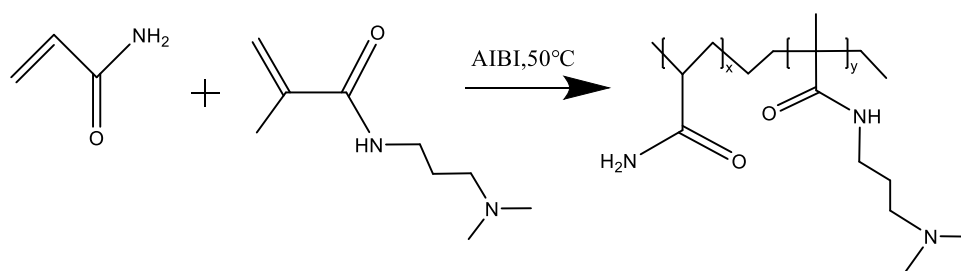


Figure 1. Chemical reaction mechanisms for the preparation of a CO₂-responsive polymer.

to obstruct large pores, diminish porous media permeability, and thereby mitigate CO₂ leakage.^{11–13} Moreover, Goodman et al. have demonstrated that a methyl methacrylate polymer sealing system displays impressive sealing prowess, enduring pressure gradients and expanding significantly at low pH levels.^{14–15} In comparison to single-ion polymers, composite gels exhibit exceptional compounded properties. A gel system combining polyacrylamide, urotropine, and resorcinol has been proposed by Li et al., where control over the gelation time and temperature is possible. This system ensures effective gel injection and responsiveness to CO₂ at formation temperatures.¹⁷ Additionally, Lashari et al. have innovatively incorporated silica particles into the R-80-HMTA-PADC system, resulting in enhanced cross-linking and structural integrity, where strength improvements have been observed.¹⁸ Therefore, the study and development of novel CO₂ sealants remain essential for advancing their efficacy that can increase the success rate of CO₂ storage technology.

Building upon the hydrolysis-swelling reaction theory and employing a reversible cross-linking polymerization approach,¹⁹ this study introduces a pioneering CO₂-responsive intelligent polymer sealant. By employing AM and DMAPMA as cross-linking monomers for CO₂-responsive polymers, coupled with PEI as the cross-linking agent, the novel sealant is formulated. This sealant exhibits the capability to polymerize in situ and dissolve in water upon solidification without affecting the liquid pH.²⁰ It offers commendable mechanical properties, specific solubility, and stability. The investigation focuses on the microstructure, rheological characteristics, and sealing performance of this innovative material, assessing various polymer and PEI compositions. The aim is to ascertain its suitability for future applications, especially in the realm of CCUS, particularly within geologic formations.

2. EXPERIMENTAL SECTION

2.1. Materials and Methods. Chemicals used in the experiments are AM (Macklin), DMAPMA (Macklin), Sorbitol (Macklin), Thoreau (Macklin), 2,2'-clay [2-(2-imidazolin-2-yl) propane] hydrochloride (AIBI, Aladdin), PEI (Sigma-Aldrich), hydrochloric acid (HCl) solution (concentration of 1.8 mol/L), ethanol, and deionized water (resistivity of 17.8 MΩ·cm).

The experimental instruments for this purpose are a Nicolet Spectran10 infrared spectrometer, a CHI760E electrochemical testing platform from Warwick Science and Technology (Wuhan) Co., Ltd., a Haake MARS III rheometer from RHEOTEST Medingen GmbH, a PerkinElmer 2000 X-ray diffractometer, and a scanning electron microscope.

2.2. Preparation of CO₂-Responsive Intelligent Polymer Blockers.

- (1) Experimental Method: Different concentrations of solutions were prepared as needed, and CO₂-responsive polymers (containing AM and DMAPMA) were used as cross-linking monomers, while polyethylene imine (PEI) was used as a cross-linking agent to prepare the cross-linked intelligent polymer blockers at room temperature.
- (2) Mechanism of Sample Preparation: By utilizing aqueous free radical copolymerization, a polymer that is responsive to CO₂ and contains protonated amine groups (-(R₂)N) as well as cross-linking groups (-NH₂) was synthesized. Subsequently, the CO₂-responsive polymer solution was cross-linked with a suitable quantity of PEI to produce a water-soluble intelligent polymer blocker (Figure 1).
- (3) The sample preparation process was as follows: different amounts of AM and DMAPMA were placed in the reaction vessel and stirred until completely dissolved.²¹ Subsequently, at 40 °C, deionized water was introduced into the mixture at a molar ratio of monomer to deionized water of 4:1, and the solution's pH was regulated to approximately 7. The mixture was then degassed with continuous N₂ until the polymerization reaction was concluded. AIBI was then added at a molar ratio of 0.5% of the monomer to initiate the polymerization reaction. The reaction proceeded for 5 h at 50 °C. Following the completion of the reaction, the product was immersed in ethanol, pulverized, and subsequently dried. Finally, the white CO₂-responsive polymer powder was obtained by allowing it to remain at 35 °C for 10 h.

A desired amount of CO₂-responsive polymer and PEI is dissolved completely in water, and then 0.5 wt % thiourea was added as a Deoxidizer. In the next step, the mixture is sealed in a flask and aged at 60 °C for 5 h to prepare the CO₂-responsive gel system. To investigate the effect of PEI on the properties of the gel, different amounts of CO₂-responsive gels were prepared, as shown in Table 1. Throughout the preparation procedure, the PEI concentration was adjusted between 0.1 and 0.6 wt %, whereas the levels of CO₂-responsive polymer (1.5 wt %) and thiourea Deoxidizer (0.50 wt %) remained the

Table 1. Polymer Systems with Different Ratios

CO ₂ responsive hydrogel	CO ₂ responsive polymer (wt %)	PEI (wt %)	thiourea (wt %)
A1	1.5	0.1	0.5
B1	1.5	0.2	0.5
C1	1.5	0.3	0.5
D1	1.5	0.4	0.5
E1	1.5	0.5	0.5
F1	1.5	0.6	0.5

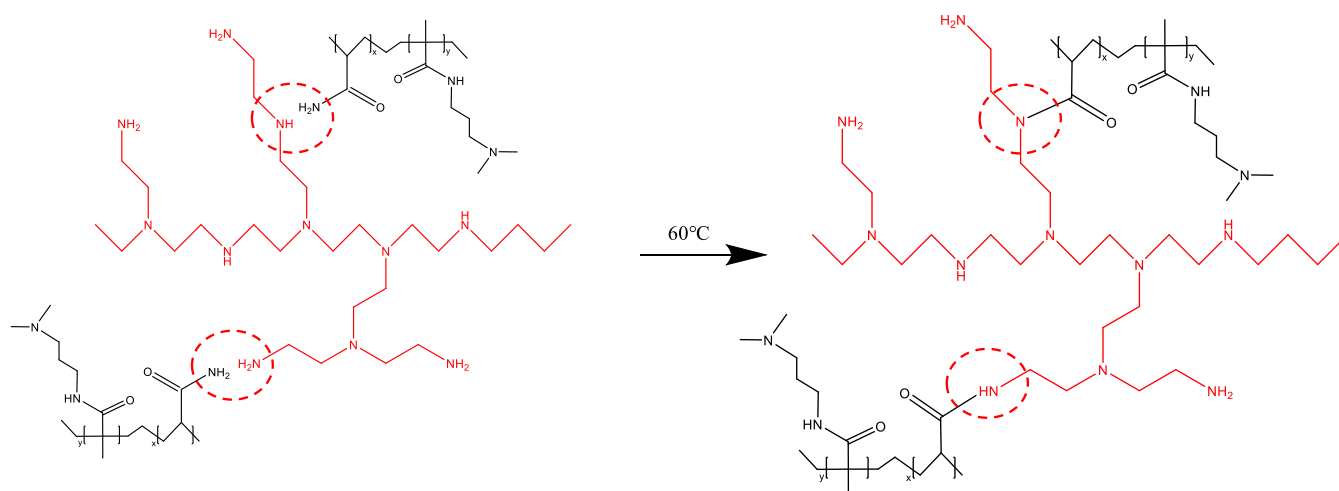


Figure 2. Chemical reaction mechanisms for the preparation of a CO₂-responsive gel.

same. Figure 2 shows the ammonia exchange reaction between amino and amide groups.^{22,23}

The prepared gel is exposed to CO₂ gas in the system, where it undergoes a sol–gel state transition. A1, B1, C1, D1, E1, and F1 represent the preresponse system, while A2, B2, C2, D2, E2, and F2 represent the postresponse system.

2.3. Characterization of Microstructure. The microstructure of this polymer system was characterized by using a scanning electron microscope. Prior to electron microscopy observation, the polymer had to be pretreated. The system was quenched rapidly in liquid nitrogen to maintain its morphology and then placed in a freeze-dryer.²⁴ The freeze-dried polymer gel systems of different categories were obtained after freeze-drying for about 72 h at $-60\text{ }^{\circ}\text{C}$. Then, a specific amount of dry sample was made into a thin slice and fixed on the sample stage with conductive adhesive. To improve the conductivity and obtain ease of observations for electron microscopy, the samples were gold-sprayed before inspections.

2.4. Thermal Properties Testing. In this experiment, the same amount of polymer sealing agent was placed separately in a ten 200 mL flask, and CO₂ was used as the reaction medium.²⁵ The system was heated at a rate of $20\text{ }^{\circ}\text{C}/\text{min}$ to $150\text{ }^{\circ}\text{C}$ in an isothermal furnace (10 KPa) and then cooled to room temperature. The response time (sol-to-gel transition time) was recorded in the temperature interval of $0\text{--}150\text{ }^{\circ}\text{C}$.

The dried and purified CO₂-responsive gel samples were powdered and pressed into pellets. Fourier transform infrared spectroscopy was performed using a Nicolet Spectran10 spectrophotometer at a resolution of 4 cm^{-1} , where the spectra were scanned 32 times, spanning from $4000\text{--}6000\text{ cm}^{-1}$.

2.5. Conductivity Testing. The experiment involved a comparison of the conductivity changes before and after the gel response to ascertain its activation. Additionally, the impact of the polymer ratio on the gel conductivity was investigated. The CHI760E electrochemical testing platform from Huawei Ke Chuang (Wuhan) Technology Co., Ltd. was used for impedance measurements of CO₂-responsive gels and preresponse polymer systems at different concentrations²⁶ (Figure S1). Platinum electrodes were used for the experiment, and conductivity data of different ratio systems were obtained and analyzed using Zview software.

The linear (low-frequency) data were obtained from gel tests, and the gel resistance was calculated using the Zview

software. It was found that the resistance value was almost equal to what it is at the intersection of the Z' axis. Therefore, this value was considered to be the true resistance property of the sample. The electrolyte conductivity of the gel can be calculated according to the following formula

$$\sigma = \frac{1}{R_s} \frac{d}{S} \quad (1)$$

where σ is the ionic conductivity, m/Ω ; R_s is the intrinsic resistance, Ω ; S is the contact area between the gel electrolyte and the electrode, m^2 ; and d is the electrode spacing, m .

2.6. Swelling Test. Dry CO₂-responsive gel samples of the same size were placed in water and exposed to CO₂ under $60\text{ }^{\circ}\text{C}$ conditions. Following a specific duration, the gel was taken out and its weight was recorded until the gel weight became stagnant. The swelling ratio (SR) was calculated based on the following expression

$$\text{SR} = \frac{W_d - W_s}{W_s} \quad (2)$$

where W_d is the weight of the gel at swelling equilibrium, kg ; and W_s is the weight of dry gel, kg .

2.7. Self-Healing Test. The self-healing time was examined in relation to the degree of mineralization, swelling ratio, and temperature. Three sets of experiments were conducted: adding an appropriate amount of C2 gel to NaCl solutions of 1–30%, adding gels with swelling ratios ranging from 10 to 30 to a 1% NaCl solution, and adding an appropriate amount of C2 gel to a 1% NaCl solution while setting different reaction temperatures between 20 and $60\text{ }^{\circ}\text{C}$. Starting from the weak bonding between particles and ending at the point where gel strength no longer increases with time, the onset and conclusion times of each set of experiments were recorded.

2.8. Rheological Evaluation. The Haake MARS III rheometer from RHEOTEST Medingen GmbH was used to evaluate the rheological performance of the polymer system before and after the response, including dynamic oscillatory shear and steady shear testing at a temperature of $60\text{ }^{\circ}\text{C}$. In dynamic oscillatory shear testing, the shear frequency ranged from 0.01 to 10 Hz, while in steady shear testing, the shear rate varied between 0.001 and 1000 s^{-1} . Finally, the effects of the

swelling ratio, mineralization degree, temperature, and CO₂ pressure on gel strength were analyzed.

2.9. Mechanical Strength Test. Prior research has solely emphasized the significance of mechanical strength in crack sealing therapy while neglecting the equally crucial adhesion behavior of gels. This is because the adhesion force plays a critical role in determining the amount of residual polymer gel volume in cracks penetrated by water or gas, while tensile and adhesion behaviors need to be studied when the CO₂-responsive gel core displacement experiments are conducted to better explain the results. Samples with similar length, width, and thickness were selected, and changes in their strength before and after CO₂-responsive gel swelling at different swelling ratios in a 1% NaCl solution were tested through tensile experiments under the CO₂ permeation conditions.

An Instron 3400 with a maximum load of 6kN was employed to perform tensile stress–strain analysis on samples that were cut into 20 × 10 × 5 mm³ sheets while maintaining a loading rate of 80 mm/min. To investigate the adhesion strength between the rock samples and the gels, peel strength tests were conducted. Specifically, a hook was fixed on one side of the rock sample with epoxy resin, while the other side was attached to the self-healing, CO₂-responsive gel. Following a three-day curing period at 60 °C, the separation force was measured with a spring balance, and the adhesion strength was then calculated using the following relationship

$$P_{\text{adhesion}} = \frac{F}{A} \quad (3)$$

where F is the maximum strength, N and A are the contact area between the gel and the rock, m².

2.10. Testing of Sealing Performance. The plugging effect of the polymer system on the cement that was used in an oil well that is highly fractured was evaluated by using the plugging rate (PR) with the F1 system (Figure S2). The plugging performance of the polymer system on gas under constant pressure displacement and the plugging performance of the polymer system on the cement were assessed using a high-temperature and high-pressure displacement device and cement, respectively.

The specific steps were as follows: saturate the cores with water, inject distilled water, and measure the steady-state pressure, flow rate, confining pressure, and permeability of the fractured rock medium for over an hour at a stable pressure and certain flow rate. Introducing CO₂ into the core to establish a gas breakthrough channel and measure the upstream pressure, flow rate, confining pressure, and permeability. Next, the polymer system is injected into the core and the upstream pressure and confining pressure. After closing the displacement device for 24 h, inject CO₂ into the core to trigger the sol–gel transition of the polymer solution, and measure the upstream pressure, flow rate, confining pressure, permeability, and plugging rate. Subsequently, distilled water was introduced into the core sample and the upstream pressure, flow rate, confining pressure, permeability, and plugging rate. Permeability was calculated using the Darcy's law

$$k = \frac{QL\mu}{A\Delta P} \quad (4)$$

where k is the absolute permeability, D; Q is the flow rate, m³/s; L is the length of the core, m; μ is the fluid viscosity, mPa·s; and ΔP is the pressure difference between the front and back

ends of the core, Pa. Since constant pressure displacement was adopted in the experiment, the outlet pressure was set as atmospheric pressure, while the upstream pressure was considered to be the injection pressure. The plugging rate was calculated using the following expression

$$PR = \frac{k_0 - k_{PR}}{k_0} \times 100\% \quad (5)$$

where k_0 is the permeability of the medium before plugging, D, while the k_{PR} is the permeability of the medium after plugging, D.

3. RESULTS AND DISCUSSION

3.1. Microstructure Analysis. In order to address the demand for CO₂-responsive polymers that are easy to prepare but possess robust stability characteristics, polymers featuring $-(R_2)N$ and $-NH_2$ that react with CO₂ were synthesized through a water-based free radical copolymerization method, as illustrated in Figure 3. The CO₂-responsive polymer was

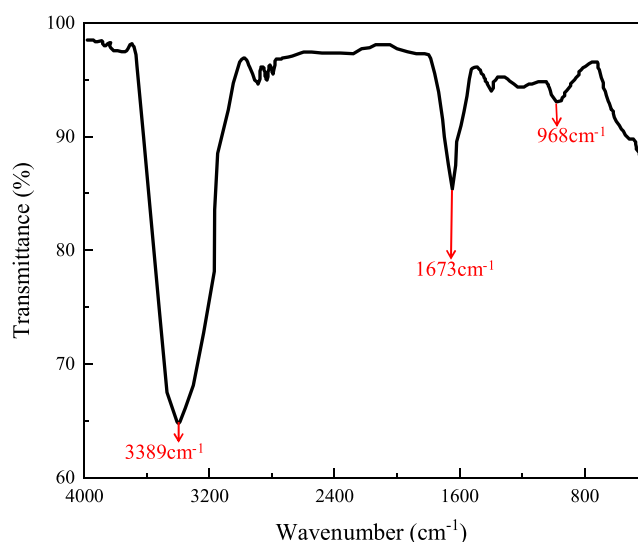


Figure 3. FT-IR spectrum of the CO₂-responsive polymer.

analyzed using FT-IR spectroscopy, with the absorption peak at 3389 cm⁻¹ indicating the presence of $-NH_2$ groups and the absorption peak at 1673 cm⁻¹ corresponding to the stretching vibration of C–O. These results confirmed that the primary monomer employed in the production of the CO₂-responsive polymer was AM. Moreover, the absorption peak observed at 968 cm⁻¹ was identified as the stretching vibration of C–N found in the tertiary amine group, thus verifying the existence of the responsive section within the CO₂-responsive polymer.

As shown in Figure 4, scanning electron microscopy analysis was performed on C1 and F1 before the response and C2 and F2 after the response and activation. The results showed that when the gel is activated, its 3D network channels are expanded, and the molecular chains are stretched, leading to volume expansion. In the system prior to the activation, the CO₂-responsive polymer had a linear structure due to the presence of the cross-linking agent, forming a CO₂-responsive gel that was relatively compact and abundant in a 3D network. Despite the fact that the CO₂-responsive gel exhibited a 3D network structure that was flexible, it was incapable of infinite expansion, like a linear polymer molecule. Given this constraint

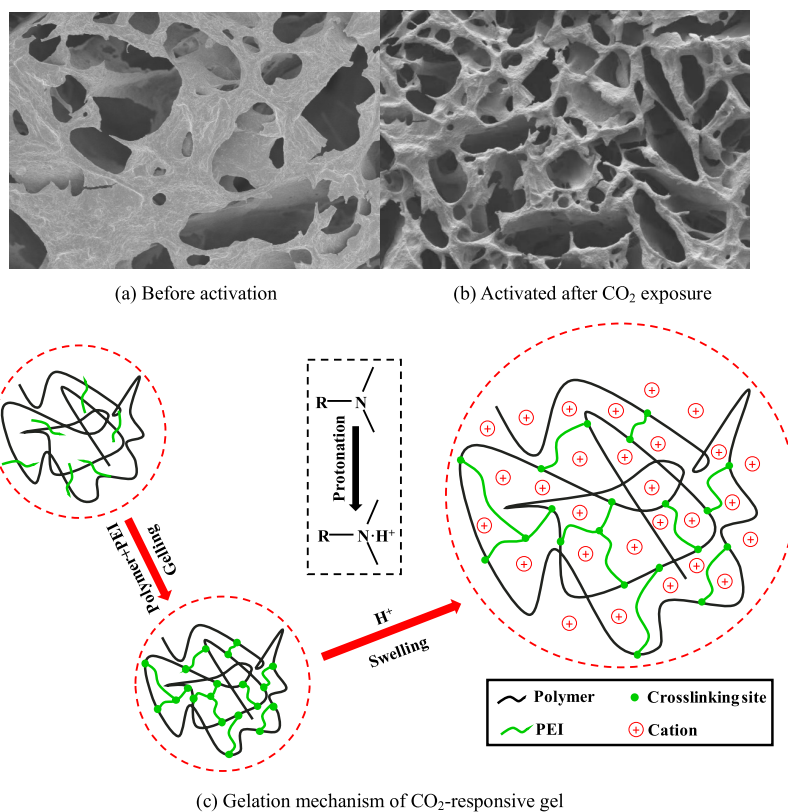


Figure 4. Microscopic morphology of the polymer system.

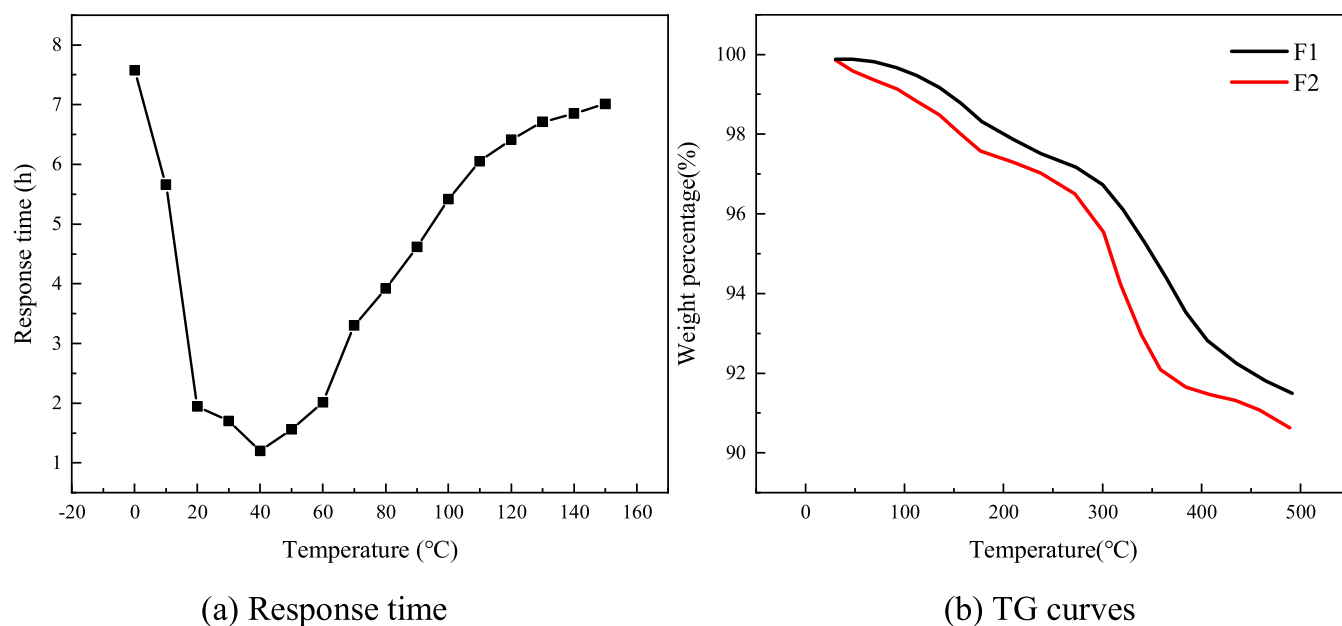


Figure 5. Results of thermal stability.

within its 3D network structure, the expansion ratio of the CO₂-responsive gel exhibited a nonpermanent nature, diminishing as the concentration of the cross-linking agent (PEI) increased.

The CO₂-responsive polymer is a polyelectrolyte complex. When CO₂ is introduced into the polymer solution system, a sol–gel transition occurs.²⁷ The gelation mechanism is shown in Figure 4, where CO₂ can bind to water molecules and dissociate H⁺ in aqueous solutions.^{28,29} In high-pressure

reservoirs, the solubility of CO₂ in formation of water increases, leading to an acidic environment due to H⁺ dissociation. The CO₂-responsive gel comprises numerous tertiary amine groups (weak bases) that can attach to H⁺. When exposed to CO₂, the CO₂-responsive gel transforms from nonionic to cationic, improving the hydrophilicity and electrostatic repulsion between polymer segments. As a result, a more uniform and complete 3D network structure is formed, resulting in greater stability of the polymer system.

3.2. Thermal Stability Analysis. Figure 5(a) shows the response time of the polymer plugging agent at different temperatures. As shown in Figure 5(a), the response time of the plugging agent at 60 °C is 2h, indicating a good response rate. The response state of the plugging agent did not change significantly over time, further demonstrating that the polymer has a good thermal stability. The thermogravimetric (TG) test results of the F1 and F2 systems are presented in Figure 5(b). When the temperature increases under 150 °C, the main weight loss is attributed to dehydration, while the weight loss rate increases between 150 and 400 °C, which may be due to the breakage of polymer chains, resulting in a large number of molecular substances being released. In the temperature range of 400–500 °C, the weight loss curve is relatively flat, denoting that the system has good temperature resistance.

3.3. Conductivity Analysis. In order to comprehensively understand variations in conductivity at various ratios of the systems, the electrochemical behavior of A2, B2, C2, D2, E2, and F2 systems was studied using AC impedance spectroscopy. The AC impedance spectra obtained are shown in Figure 6,

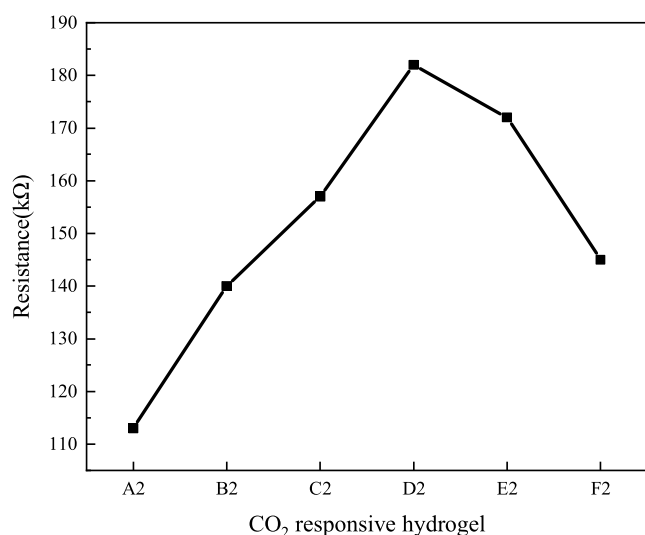


Figure 6. Resistance of different CO₂-responsive gel systems.

where the resistance values of A2, B2, C2, and D2 systems gradually increased, signifying that the conductivity is decreasing. Starting from the E2 system, however, the resistance value begins to decrease gradually, representing that the conductivity is increasing. This is because the conductivity of the polymer system is related to the ratio of positive and negative ions on the polymer chain due to the electrostatic attraction between them.

When the system is activated by being exposed to CO₂, the number of positive charges in the A, B, C, and D polymer systems increases, combining with the negative charges, and the overall charge decreases, resulting in a gradual decrease in conductivity. Conversely, the E system contains more cross-linking agents (PEI), making the 3D network structure of the gel too tight and reducing its hydrophilicity. Therefore, after CO₂ exposure and activation, the amount of H⁺ absorbed by the system decreases and the negative ions neutralized would decrease as well, while the relative amount of negative charge increases, leading to a gradual increase in the conductivity of the system.

3.4. Swelling Performance Analysis. Various gel networks should have different water absorption capacities and swelling abilities, which can be considered an important indicator of the overall gel performance. As presented in Figure 7, with the increase of PEI concentration, the swelling ratio of

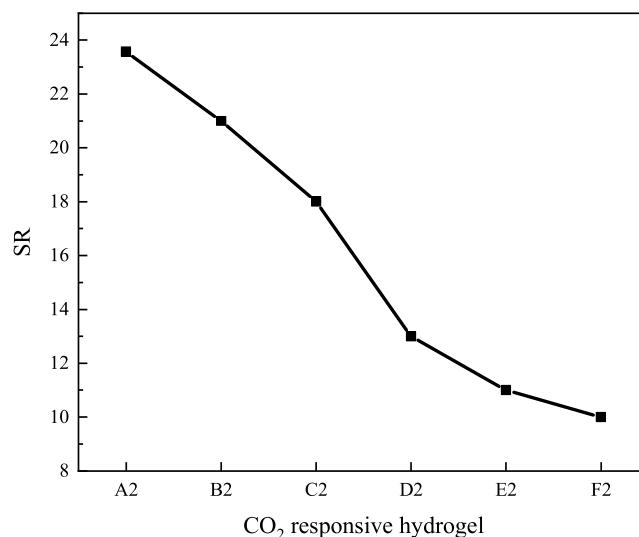


Figure 7. Changes in the SR of the gel in an aqueous solution that contains CO₂.

the gel gradually decreases. This is attributed to the introduction of an ion cross-linking network that enhances the physical cross-linking density inside the gel but improves the strength of the gel, which also makes the spatial network structure tighter. Therefore, the swelling ratio of the gel decreases significantly. It should be noted that in the aqueous solution that contains CO₂, the swelling ratio of the gel can still reach 10–24, which is considered an excellent mechanical property.

3.5. Self-Healing Performance Analysis. Considering Figure 8(a), the onset and end of the self-healing time are delayed with the increasing degree of mineralization. Experimental results explain that when the gel particles are in a 1% NaCl solution, the self-healing begins after 2 h, and it takes 4 days of curing at room temperature for the gel strength to reach a constant value. In a 30% NaCl solution, it takes 10 h for the gel particles to start self-healing, and it takes 10 days of curing at room temperature for the gel strength to remain constant. This is because the high mineralization degree hinders the self-healing speed and delays the gel swelling process.³⁰ Moreover, the diffusion rate of the secondary cross-linking agent in high mineralization degree solutions is restricted due to the charge shielding effect and low stretching degree of the polymer network structure. As depicted in Figure 8(b), it was observed that the initial and final self-healing times decrease with an increase in the swelling ratio in a 1% NaCl solution. At a swelling ratio of 10, gel particles initiate self-healing after 2 h, and the gel strength stabilizes after 4 days of curing at room temperature. By increasing the swelling ratio to 30, the final self-healing time can be reduced to 3.1 days. Additionally, Figure 8(c) illustrates that the self-healing time decreases progressively as the temperature rises. When the temperature increases from 20 to 60 °C, the onset of self-healing decreases from 120 to 90 min, while the ending time reduces from 4 to 2.5 days.

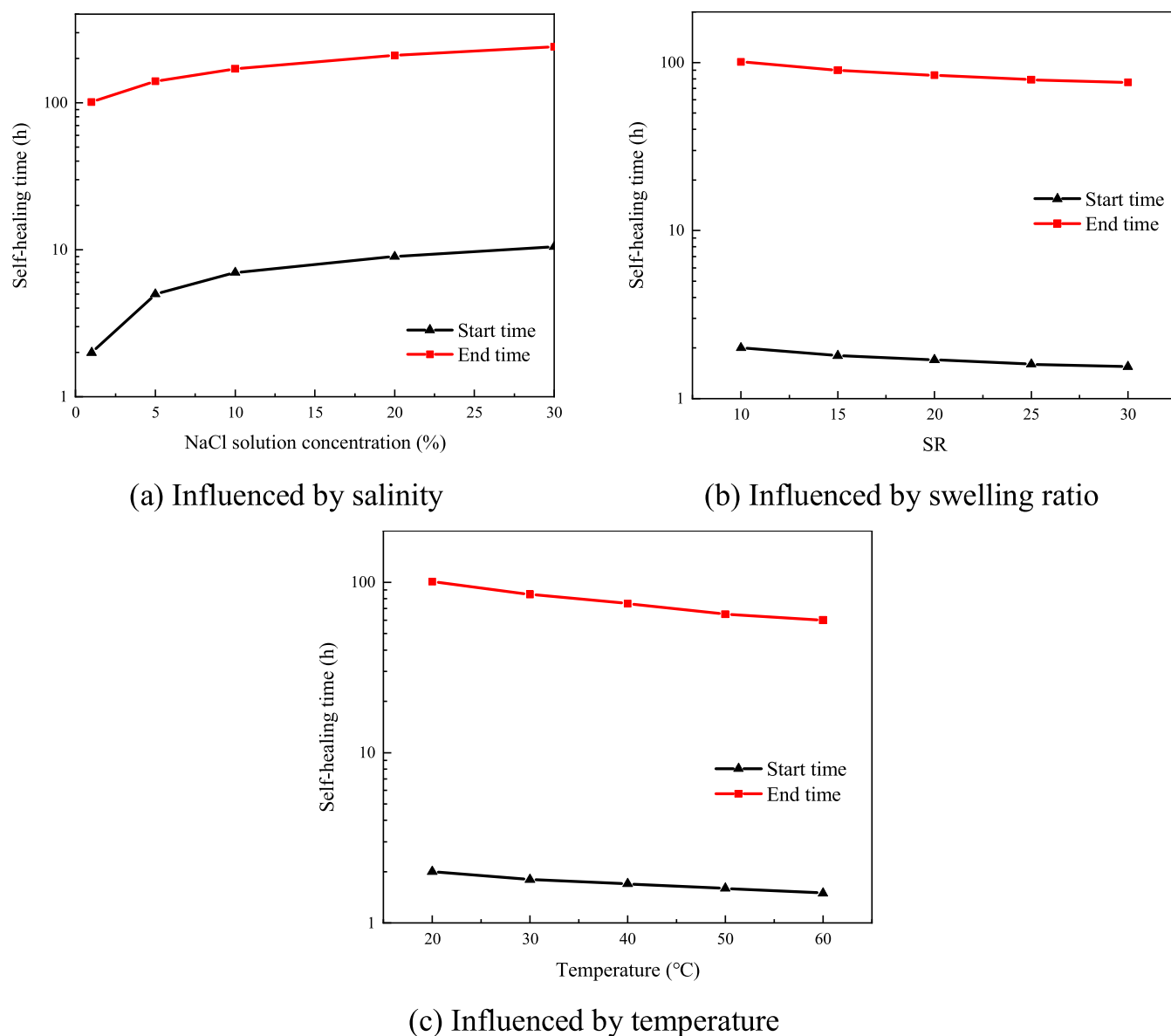


Figure 8. Self-healing time.

3.6. Rheological Property Analysis. Based on the steady-state shear curve in Figure S3, we can obtain the relationship between the preresponse shear viscosity (η) of the polymer system and the shear rate. According to the experimental results, it was observed that for various polymers and different PEI mass fractions, the shear viscosity progressively decreases as the shear rate increases, implying that the system behaves like a pseudoplastic fluid. Additionally, at the same shear rate, the shear thinning effect of the system becomes more pronounced with an increasing PEI mass fraction. This is because as the shear rate increases, the status of polymer chains would transform from being mutually intertwined or coiled during a stationary state to being oriented in the flow direction, leading to a reduction in internal resistance where they start to exhibit a decrease in viscosity at the macroscale. The viscosity of A1 exhibits a sharp decline at a shear rate of 10 s^{-1} , possibly due to the shear rate that has already destroyed the physical entanglement of the existing two kinds of polymers in the system, causing the polymer chains to stretch out from their original coiled state, thereby reducing the resistance between

molecular chains and exhibiting a decrease in viscosity at the macroscale. In addition, the concentrations of CO_2 -responsive polymer and thiourea deoxidant in A1 and D1, B1 and E1, and C1 and F1 are both quantitative. The experimental data show that with an increase in PEI mass fraction in the system, the viscosity of the entire system significantly increases. This can be related to the 3D network of the gel that becomes denser with an increase in the PEI content. At shear rates ranging from 100 to 1000 s^{-1} , the viscosity of A1, B1, C1, D1, E1, and F1 is between 2 and $100 \text{ mPa}\cdot\text{s}$, specifying that the polymer system before the response owns a suitable injectability.

Based on the experimental data in this study, the following expression was used for fitting the data

$$\tau = K \cdot \dot{\gamma} \quad (6)$$

where τ is the flow shear stress, Pa; K is the consistency coefficient, $\text{Pa}\cdot\text{s}^n$; $\dot{\gamma}$ is the shear rate, s^{-1} ; n is the flow behavior index, which is used to determine the degree to which the fluid deviates from the Newtonian fluid. The greater the consistency coefficient of the system, the higher the viscosity and the more

viscous the state at the macro level would become, and thus, the output after the steady-state shear conditions comprises flow shear stress.

After fitting of the experimental data, parameters in Table 2 are obtained. From the results, it can be seen that this polymer

Table 2. Polymer Systems with Different Ratios

polymer system	shear rate (s^{-1})	K ($Pa \cdot s^n$)	n	fluid type
A1	0.005–1000	0.61863	0.12943	pseudoplastic fluid
B1	0.005–1000	0.04896	0.67435	pseudoplastic fluid
C1	0.005–1000	0.26834	0.58324	pseudoplastic fluid
D1	0.005–1000	3.89454	0.15893	pseudoplastic fluid
E1	0.005–1000	0.31534	0.58346	pseudoplastic fluid
F1	0.005–1000	0.02974	0.88342	pseudoplastic fluid

system exhibits the characteristics of a pseudoplastic fluid, where the viscosity gradually decreases as the shear rate increases. At the same time, it is observed that the smaller the n value, the slower the trend of increasing resistance between the polymer chains, and the lower internal molecular binding force due to structural damage would be expected. Therefore, we can conclude that the viscosity of the system significantly decreases under high shear rates, which also explains the previous experimental data showing a decrease in viscosity with an increase in shear rate.

This section studies the oscillatory rheological curves of the storage modulus (G_1) and loss modulus (G_2) of the polymer systems at different shear frequencies (f), as shown in Figure 9(a). In dynamic oscillatory testing, G_1 and G_2 represent the elasticity and viscosity of the system, respectively.³¹ Experimental results show that with the increase of PEI mass fraction

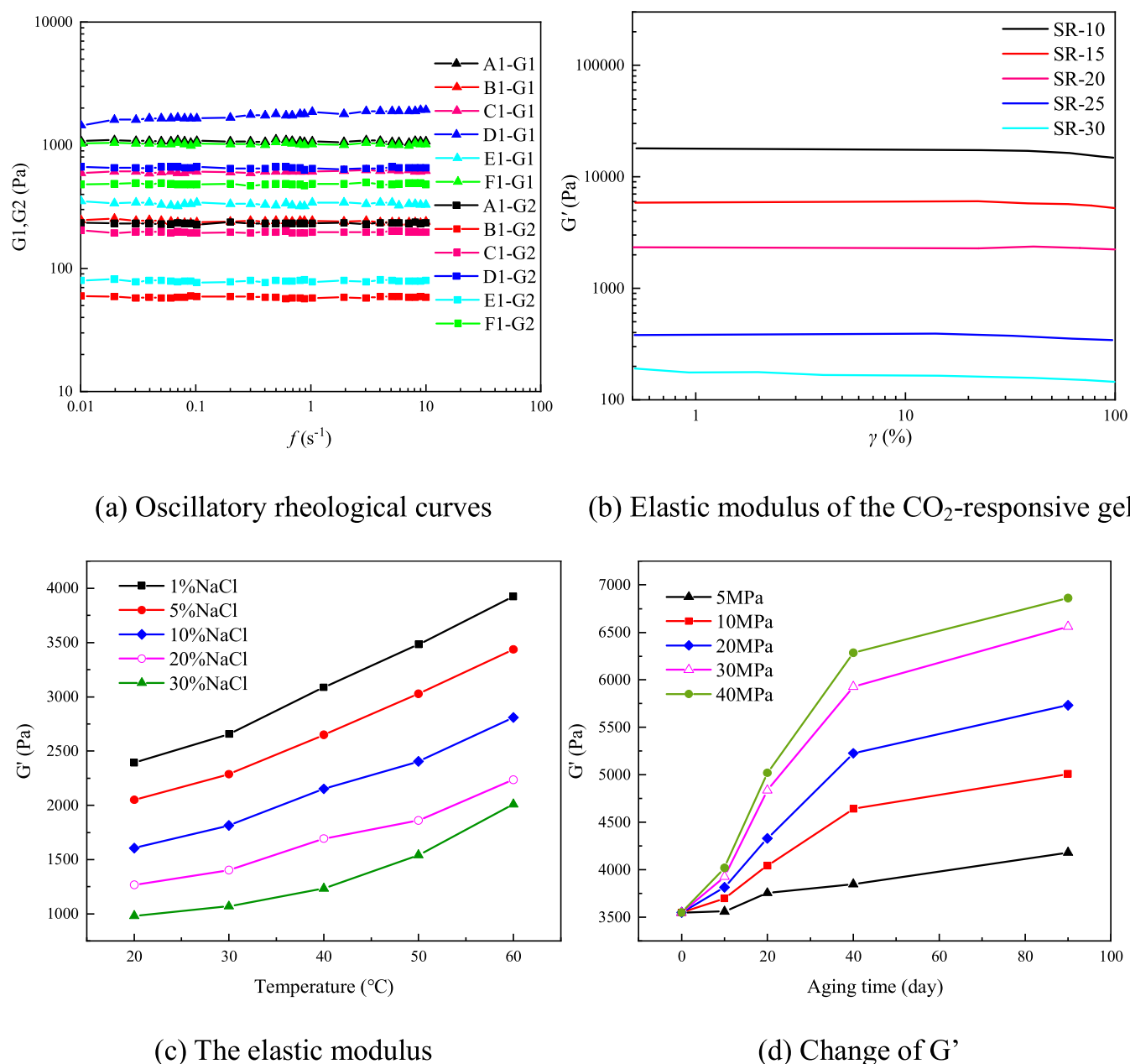


Figure 9. Results of rheological property.

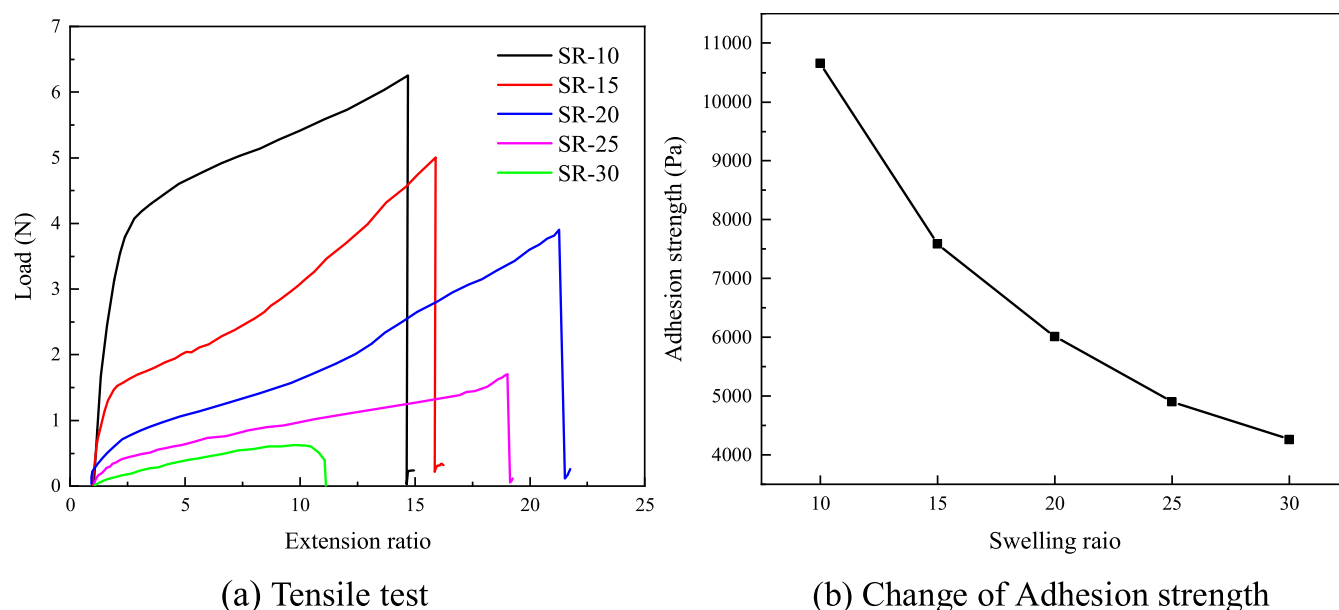


Figure 10. Results of stretching and adhesion performance.

Table 3. Plugging Performance of CO₂-Responsive Smart Polymer (60 °C)

step	injected fluid	injection pressure (MPa)	flow rate (mL/min)	confining pressure (MPa)	permeability 10 ⁻³ μm ²	plugging rate (%)
1	distilled water	5.18	0.06	36	0.009862	
2	CO ₂	27.46	0.17	36	0.006397	
3	polymer solution	32.78		39		
4	CO ₂	33.17	0.03	39	0.002604	73.6
5	distilled water	34.83	0.01	40	0.000374	96.2

in the system, the modulus first decreases and then increases. This is due to the increase of PEI that is used results in improved physical cross-linking between the two polymers in the system; thus, the water retention ability of the system is enhanced, which leads to a decrease in the modulus. That is, the increase in the water retention capacity of the gel will decrease the mechanical performance of the system. With further increase of PEI usage, the physical cross-linking between the two polymers in the system becomes tighter, and the increase in the strength of the polymer network outweighs the increase in the water retention ability of the system. The G₂ values of A1 to E1 are greater than G₁, while G₁ and G₂ both increase with frequency, which is a typical characteristic of gel systems with covalent bonds and physical cross-linking.³² The G₁ value of F1 was measured larger than that of G₂, signifying that with the increase of mass fraction of these two polymers, electrostatic interaction increases further, leading to an increase in the modulus of the system. It is speculated that the F system forms a 3D network during shearing, thus giving the advantage to G₁. With consideration: Figure 9(a), it can be concluded that the modulus of the gel polymers is not significantly affected by shear frequency, maintaining a relatively stable state and confirming that the gel is strong with acceptable strength.

We further assessed the elastic modulus (G') of the gel based on the tests that were conducted in the linear viscoelastic range. Based on Figure 9(b), it is observed that the increase of swelling ratio will cause a decrease in the strength of the gel. It can be seen from Figure 9(c) that the gel strength decreases as the degree of mineralization increases. For instance, in a 30%

NaCl solution, the gel strength remains high at 986 Pa and increases significantly with temperature.

This study evaluated the change in the strength of the gel vs CO₂ exposure time and pressure by CO₂ stability testing, as presented in Figure 9(d). The results imply that the exposure time and pressure have a positive impact on the gel strength. When the pressure is 40 MPa, the gel strength almost doubles after 90 days. In addition, during the degassing process, the polymer gel swelled and formed a porous foam, and the gel strength slightly increased after the gel was taken out of the container. This is because, during degassing, CO₂ expands and comes out to produce bubbles, generating a porous network structure that enhances the gel strength.

3.7. Analysis of Stretching and Adhesion Performance. The mechanical performance of the gel was evaluated through tensile testing, and the results are shown in Figure 10. The maximum loading pressure of the gel with a swelling ratio less than 25 reached more than 1.5N, which proves that the gel has excellent mechanical strength and elasticity.

Moreover, the adhesion strength of the gel was characterized using the peel strength, and the results are displayed in Figure 10. The findings revealed that the adhesion strength decreased gradually as the swelling ratio increased, decreasing from 10660 Pa (SR = 10) to 4264 Pa (SR = 30). This phenomenon can be attributed to the decrease in polymer concentration resulting from the increased swelling ratio, which leads to the dilution of the entangled structure and excessively lower modulus values, causing the material to easily flow and lose its adhesion force.³³ The adhesion strength of the gel is higher when the swelling ratio is low, denoting the desired applicability of the gel when it is injected into porous rocks.

3.8. Plugging Performance Analysis. According to the data presented in Table 3, the plugging rate of the polymer system to CO₂ is 73.6% and to water is 96.2%. The injection pressure difference of deionized water and CO₂ before and after the polymer system was injected into the sample changed significantly. Herein, the injection pressure of the water phase increased from 5.18 to 34.83 MPa, while the injection pressure of the gas phase increased from 27.46 to 33.17 MPa. This suggests that the gel can effectively plug the fractured core and owns suitable plugging abilities.

4. CONCLUSIONS

In this study, a new type of smart polymer plugging agent with self-healing and water solubility characteristics was introduced, and its properties were evaluated. Based on the results, the following conclusions can be drawn:

- (1) The new polymer encompasses multiple tertiary amine groups (weak bases) capable of H⁺ binding, which can react with CO₂ to form a uniform, complete 3D network structure, fulfilling the intelligent response feature to CO₂.
- (2) The polymer has desirable rheological properties, and the structural state of its molecular chain under shear stress can achieve proper dilution performance. By changing the amount of PEI and the salinity of the saline water, the rheological viscosity and self-healing rate of the polymer can be adjusted to improve its plugging efficiency.
- (3) The polymer also shows notable plugging performance where a nanogel structure was formed after it is dissolved in water that can effectively protect the pore surface and improve its compressive strength. Under the condition of a swelling ratio of 30, its tensile strength reached 0.65N, and the adhesion capacity of 4264 Pa was achieved, which makes it a suitable candidate to mitigate the risk of CO₂ escaping from the fractures.

■ ASSOCIATED CONTENT

SI Supporting Information

The Supporting Information is available free of charge at <https://pubs.acs.org/doi/10.1021/acsomega.3c04466>.

The contents of testing devices and steady-state shear curves are supplied as Supporting Information (PDF)

■ AUTHOR INFORMATION

Corresponding Author

Huimei Wu – National Engineering Research Center for Oil & Gas Drilling and Completion Technology, Yangtze University, Wuhan 430100, China; Hubei Key Laboratory of Oil and Gas Drilling and Production Engineering, Yangtze University, Wuhan 430100, China; orcid.org/0009-0006-3957-3510; Email: wuhuimei@yangtzeu.edu.cn

Authors

Yishan Lou – National Engineering Research Center for Oil & Gas Drilling and Completion Technology, Yangtze University, Wuhan 430100, China; Hubei Key Laboratory of Oil and Gas Drilling and Production Engineering, Yangtze University, Wuhan 430100, China

Xiaopeng Zhai – National Engineering Research Center for Oil & Gas Drilling and Completion Technology, Yangtze University, Wuhan 430100, China; Hubei Key Laboratory of

Oil and Gas Drilling and Production Engineering, Yangtze University, Wuhan 430100, China

Zhonghui Li – National Engineering Research Center for Oil & Gas Drilling and Completion Technology, Yangtze University, Wuhan 430100, China; Hubei Key Laboratory of Oil and Gas Drilling and Production Engineering, Yangtze University, Wuhan 430100, China

Bin Liu – National Engineering Research Center for Oil & Gas Drilling and Completion Technology, Yangtze University, Wuhan 430100, China; Hubei Key Laboratory of Oil and Gas Drilling and Production Engineering, Yangtze University, Wuhan 430100, China

Complete contact information is available at:

<https://pubs.acs.org/10.1021/acsomega.3c04466>

Notes

The authors declare no competing financial interest.

■ ACKNOWLEDGMENTS

This work was supported by the National Natural Science Foundation of China (U19B6003-05).

■ REFERENCES

- (1) Luo, X. J.; Zheng, P. F.; Gao, K.; Wei, B.; Feng, Y. J. Thermo- and CO₂-triggered viscosifying of aqueous copolymer solutions for gas channeling control during water-alternating-CO₂ flooding. *Fuel* **2021**, *291*, 120171.
- (2) Kutchko, B. G.; Strazisar, B. R.; Dzombak, D. A.; Lowry, G. V.; Thaulow, N. Degradation of well cement by CO₂ under geologic sequestration conditions. *Environ. Sci. Technol.* **2007**, *41*, 4787–4792.
- (3) Pu, W. F.; Du, D. J.; Fan, H. C.; Chen, B. W.; Yuan, C. D.; Varfolomeev, M. A. CO₂-responsive preformed gel particles with interpenetrating networks for controlling CO₂ breakthrough in tight reservoirs. *Colloids Surf., A* **2021**, *613*, No. 126065.
- (4) Hui-Min, Z.; Lin, D.; Yang, G.; Chun, Y.; Xu, Q. H. Adsorption capacity of carbon dioxide on amine modified mesoporous materials with larger pore sizes. *Acta Phys-Chim Sin.* **2012**, *28*, 985–992.
- (5) Wang, J.; Liu, H.; Ning, Z.; Zhang, H. Experimental research and quantitative characterization of nitrogen foam blocking characteristics. *Energy Fuels* **2012**, *26*, 5152–5163.
- (6) Wei, B.; Li, Q.; Jin, F.; Li, H.; Wang, C. The potential of a novel nano-fluid in enhancing oil recovery. *Energy Fuels* **2016**, *30*, 2882–2891.
- (7) Tavassoli, S.; Ho, J. F.; Shafiei, M.; Huh, C.; Bommer, P.; Bryant, S.; Balhoff, M. T. An experimental and numerical study of wellbore leakage mitigation using pH triggered polymer gelant. *Fuel* **2018**, *217*, 444–457.
- (8) Li, D.; Zhang, L.; Ren, S.; Rui, H. Leakage mitigation during CO₂ geological storage process using CO₂ triggered gelation. *Ind. Eng. Chem. Res.* **2019**, *58*, 3395–3406.
- (9) Shen, H.; Yang, Z.; Li, X.; Peng, Y.; Lin, M.; Zhang, J.; Dong, Z. CO₂-responsive agent for restraining gas channeling during CO₂ flooding in low permeability reservoirs. *Fuel* **2021**, *292*, No. 120306.
- (10) Chen, Y.; Zhao, T.; Wang, B.; Qiu, D.; Ma, N. Highly sensitive CO₂-responsive polymeric microgels that respond within seconds. *Langmuir* **2015**, *31*, 8138–8145.
- (11) Durucan, S.; Korre, A.; Shi, J. Q.; Govindan, R.; Mosleh, M. H.; Syed, A. The use of polymer-gel solutions for CO₂ flow diversion and mobility control within storage sites. *Energy Procedia* **2016**, *86*, 450–459.
- (12) Syed, A.; Pantin, B.; Durucan, S.; Korre, A.; Shi, J. Q. The use of polymer-gel solutions for remediation of potential CO₂ leakage from storage reservoirs. *Energy Procedia* **2014**, *63*, 4638–4645.
- (13) Mosleh, M. H.; Govindan, R.; Shi, J. Q.; Durucan, S.; Korre, A. The use of polymer-gel remediation for CO₂ leakage through faults and fractures in the caprock. *Energy Procedia* **2017**, *114*, 4164–4171.

- (14) Goodman, H.; Espie, T.; Minnig, C.; Rösli, U.; Gisiger, J.; Roback, R. *Testing Advanced Sealants to Address Wellbore Seepage of CO₂ Behind Casing at the Mont Terri Underground Research Laboratory, 14th Greenhouse Gas Control Technologies Conference*. Melbourne, Australia 2018.
- (15) Li, D.; Zhang, L.; Ren, B.; Ren, S. Experimental study of CO₂-sensitive chemicals for enhanced sealing of leakage pathways in CO₂ geological storage process. *Energy Procedia* **2014**, *63*, 4646–4657.
- (16) Li, D. X.; Zhang, L.; Liu, Y. M.; Kang, W. L.; Ren, S. R. CO₂-triggered gelation for mobility control and channeling blocking during CO₂ flooding processes. *Pet. Sci.* **2016**, *13*, 247–258.
- (17) Li, D.; Zhang, L.; Ren, S.; Rui, H. Leakage mitigation during CO₂ geological storage process using CO₂ triggered gelation. *Ind. Eng. Chem. Res.* **2019**, *58*, 3395–3406.
- (18) Lashari, Z. A.; Yang, H.; Zhu, Z.; Tang, X.; Cao, C.; Iqbal, M. W.; Kang, W. Experimental research of high strength thermally stable organic composite polymer gel. *J. Mol. Liq.* **2018**, *263*, 118–124.
- (19) Jiang, K.; Ashworth, P. The development of Carbon Capture Utilization and Storage (CCUS) research in China: A bibliometric perspective. *Renewable Sustainable Energy Rev.* **2021**, *138*, No. 110521.
- (20) Tapia, J. F. D.; Lee, J. Y.; Ooi, R. E.; Foo, D. C.; Tan, R. R. A review of optimization and decision-making models for the planning of CO₂ capture, utilization and storage (CCUS) systems. *Sustainable Prod. Consumption* **2018**, *13*, 1–15.
- (21) Yan, Y. L.; Borhani, T. N.; Subraveti, S. G.; Pai, K. N.; Prasad, V.; Rajendran, A.; Nkulikiyinka, P.; Asibor, J. O.; Zhang, Z. E.; Shao, D.; et al. Harnessing the power of machine learning for carbon capture, utilisation, and storage (CCUS)-a state-of-the-art review. *Energy Environ. Sci.* **2021**, *14*, 6122–6157.
- (22) Ghriga, M. A.; Khoukh, A.; Lebouachera, S. E. I.; Grassl, B. NMR investigation on the thermogelation of partially hydrolysed polyacrylamide/polyethylenimine mixtures. *Soft Matter* **2022**, *18*, 7075–7081.
- (23) Song, T.; Bai, B.; Eriyagama, Y.; Schuman, T. Lysine Crosslinked Polyacrylamide- A Novel Green Polymer Gel for Preferential Flow Control. *ACS Appl. Mater. Interfaces* **2023**, *15*, 4419–4429.
- (24) Vishal, V.; Chandra, D.; Singh, U.; Verma, Y. Understanding initial opportunities and key challenges for CCUS deployment in India at scale. *Resour., Conserv. Recycl.* **2021**, *175*, No. 105829.
- (25) Fukai, I.; Mishra, S.; Pasumarti, A. Technical and economic performance metrics for CCUS projects: Example from the East Canton Consolidated Oil Field. *Energy Procedia* **2017**, *114*, 6968–6979.
- (26) Liu, D. F.; Luo, R.; Nie, J.; Guan, W. C. Characterizations of a branched ester-type lithium imide in methoxy ether-substituted poly (organophosphazenes)-based solid polymer electrolytes. *Mater. Sci. Eng.: B* **2005**, *119*, 99–104.
- (27) Kwon, I. C.; Bae, Y. H.; Kim, S. W. Electrically erodible polymer gel for controlled release of drugs. *Nature* **1991**, *354*, 291–293.
- (28) Wang, X.; Pan, L.; Wu, K.; Li, L.; Xu, J.; Lau, H. C. Experiment based modeling of CO₂ solubility in H₂O at 313.15–473.15 K and 0.5–200 MPa. *Appl. Geochem.* **2021**, *130*, No. 105005.
- (29) Someya, S.; Bando, S.; Chen, B.; Song, Y.; Nishio, M. Measurement of CO₂ solubility in pure water and the pressure effect on it in the presence of clathrate hydrate. *Int. J. Heat Mass Transfer* **2005**, *48*, 2503–2507.
- (30) Sircar, S.; Keener, J. P.; Fogelson, A. L. The effect of divalent vs. monovalent ions on the swelling of mucin-like polyelectrolyte gels: governing equations and equilibrium analysis. *J. Chem. Phys.* **2013**, *138*, 145–156.
- (31) Ying-Hua, S.; Liu, H. M.; Li, G. Q.; Zhai, Z. G.; Shu, X. F.; Tai, X. M. Rheological Properties and Gelation of pH-Responsive P(HEMA/MAA) Nano-Microgel Dispersions. *Acta Phys.-Chim. Sin.* **2011**, *27*, 1919–1925.
- (32) Park, S.; Edwards, S.; Hou, S.; Boudreau, R.; Yee, R.; Jeong, K. J. A multi-interpenetrating network (IPN) hydrogel with gelatin and silk fibroin. *Biomater. Sci.* **2019**, *7*, 1276–1280.
- (33) Dompé, M.; Vahdati, M.; van Ligten, F.; Ligten, F. V.; Cedano-Serrano, F. J.; Hourdet, D.; Creton, C.; Zanetti, M.; Bracco, P.; van der Gucht, J.; Gucht, J. V. D.; Kodger, T. Enhancement of the Adhesive Properties by Optimizing the Water Content in PNIPAM-Functionalized Complex Coacervates. *ACS Appl. Polym. Mater.* **2020**, *2*, 1722–1730.